DOI: 10.13009/EUCASS2017-545

Trajectory Optimization of Commom Aero Vehicle through Genetic Algorithm aided with Rational Bézier Curve

Usman Fareed[⋆,†]*, Ke Zhang*[⋆,†] *and Mir Soban Ahmed*[⋆,†]
[⋆]*School of Astronautics, Northwestern Polytechnical University, Xi'an, P.R.China*
[†] *National Key Laboratory of Aerospace Flight Dynamics, School of Astronautics, Xi'an, P.R.China*
usmanfareed07@yahoo.com · zhangke@nwpu.edu.cn · soban@mail.nwpu.edu.cn

Abstract

The requirement of computing optimized entry trajectory for Common Aero Vehicle (CAV) satisfying both path constraints and terminal constraints has been widely debated since, the development of CAV by the Boeing for USA FALCON program. Proposed novel approach generates optimized guidance command in terms of bank angle (σ) for hypersonic reentry weapon platform, through conventional genetic algorithm aided with rational bézier curve. The control points are defined in terms of latitude, longitude and radial distance along with the weight factor associated with each control point. Fitness function as trajectory constraints is minimized by genetic algorithm. Rational bézier uses optimized control points and weight factors to generates state differentials. The derivatives of the states w.r.t the bézier time t_b, behaves as a new dynamic model of CAV. Finally, the actual optimized trajectory of CAV in flight time t, is regenerated using interpolated value of bank angle σ from bézier command of σ_b. Desired path constraints are the controlled values of heating rate Q, dynamic pressure q and normal loading n. Terminal constraints provided by terminal area attack management (TAAM) guidance system are acceptable error bound for terminal flight path angle, azimuth angle, velocity and TAAM entry point. Finally, the evaluation of proposed method is demonstrated by modeling comparative simulations against GPOPS-II matlab software.

1. Introduction

In order to sustain and enhance the national security, need of long range strike capability come up after military analysts discussed the shortcomings of past wars situations. Prompt Global Strike PGS in Yong et al[3] established the requirement for a system that can deliver a precision-guided speedy conventional worldwide air strike. For this reason DARPA Falcon in Sachdev et al,[16] a two part joint project has been launched between Defense Advanced Research Projects Agency DARPA and the United States Air Force USAF which is a part of PGS. One of the aspects of above mentioned goal is to have a global strike capability George et al[8] using hypersonic cruise vehicle Walker et al,[17] where targets within a 9,000 nautical mile range can be reached in less than two hours. Thus, the focus in current researches is on the development of a common aerial platform (*CAV*) in George et al[7] for hypersonic Intercontinental Ballistic Missiles ICBMs and cruise missiles, as well as civilian Reusable Launch Vehicles RLVs and Expendable Launch Systems ELVs. The trajectory optimization of CAV to meet mission specific requirements is the part of our proposed research.
Trajectory optimization of CAV with hypersonic initial speed along with handling path constraints and terminal constraints is a challenging task. Direct solution methods Betts et al[2] have been extensively used for solving the variety of trajectory optimization problem. Gauss Pseudo-spectrum method and the Legendre Pseudo-spectrum method in Fariba et al[5] have improved the calculation efficiency remarkably, these algorithms still have bigger distance to the on board applications, especially in terms of calculation efficiency when dealing with on board flight constraints investigated by Zhang et al.[21] Legendre Pseudo-spectrum method in Rao et al[1] was implemented by many researchers and they also have implemented Chebyshev pseudospectral method in Fahroo et al[4] for directly solving a generic Bolza optimal control problem with state and control constraints.
Number of modified pseudospectral methods have been implemented to minimize computation time associated with large number of discrete points in traditional pseudospectral method. Multistage pseudospectral method[11] . The performance of the multistage pseudospectral method is demonstrated by numerical examples of the free-space flight, target transition flight, and threat avoidance flight. Jinglin et.al.[18] proposed radau pseudospectral method to solve optimal control problem by dividing HCV trajectory into phases and modifies dynamic model using trajectory damping control technique to enhance damping of the trajectory and compared it with Gauss Pseudo spectral method.

DOI: 10.13009/EUCASS2017-545

Easy Gauss Pseudo spectral method EGPM[22] has been used to solve two examples using modified data of CAV. Firstly the author maximize the downrange without path constraints and use GPOPS for comparison. In second example, they have generated the multi phase trajectory which satisfies the Way-points and No-fly zone constraints. Evolutionary algorithms like genetic and particle swarm optimization algorithms have also been used to solve complex constraints for HCVs trajectory optimization.[19] has applied particle swarm method for trajectory optimization of CAV-H and compared the results with artificial fish algorithm. Their results show that by the help of numerical simulations the swarm intelligence algorithms are suitable for the large-scale, complex, and nonlinear trajectory optimization problem.
Yokoyama et al[20] proposed a numerical trajectory optimization method using a real-coded genetic algorithm in order to find an initial solution to gradient-based direct trajectory optimization. Though, the convergence properties of their method are receptive to the penalty parameter. They applied their method to constrained brachistochrone problem and a space plane reentry problem. In the end, their proposed technique performed well in both characteristic.
Model Predictive Static Programming MPSP by Omkar et al[9] has been used to solve trajectory optimization for HCV, but the initial guess of control variables i-e angle of attack (α) and side slip angle (σ) is required for MPSP to proceed. Convergence time in MPSP algorithm becomes very large, if the initial guess of control variables is not accurate. Secondly this method cannot handle path constraints. The path constraints are handled by dividing the whole trajectory into parts, and patched based trajectory solution is provided to achieve trajectory path constraints. Over all, MPSP is a novel approach to provide smooth trajectory with minimum control energy requirement to get terminal constraints effectively.
A novel approach using evolutionary genetic algorithm aided with rational bézier curve Farin et al[6] is presented here to achieve optimized trajectory for CAV. Performance index is the function of trajectory constraints where as terminal TAAM entry point is ensured though last control point of rational bézier curve. These optimized control points are used to reconstruct CAV trajectory in bézier domain. Control variable from bézier domain interpolated to flight time domain, to be used as an input to the actual dynamic model of CAV.
The comparison of the proposed method for CAV trajectory optimization has been done with the GPOPS-II in Patterson et al,[13] which is a general-purpose MATLAB software for solving multiple phase optimal control problems. The software employs a Legendre Gauss Radau (LGR) quadrature orthogonal collocation method where the continuous-time optimal control problem is transcribed to a large sparse nonlinear programming problem (NLP). An adaptive mesh refinement method is implemented that determines the number of mesh intervals and the degree of the approximating polynomial within each mesh interval to achieve a specified accuracy.

2. Preliminaries

CAV dimensionless model, pseudo code for genetic algorithm along with the mathematical details for n^{th} order rational bézier curve shall be the part of this section. These are the prerequisite in order to compute the optimized trajectory of CAV using genetic algorithm aided with rational bézier curve. The necessary details associated with each model is explained below.

2.1 Common Aero Vehicle Mathematical Model

Three dimensional point mass simulation of common aero vehicle is implemented using dynamic model of common aero shell described by Zuojun et al.[15] The dimensionless equation of motion using spherical rotating earth model is formulated as

$$\dot{r} = V sin\gamma \tag{1}$$

$$\dot{\theta} = \frac{V cos\gamma sin\psi}{r cos\phi} \tag{2}$$

$$\dot{\phi} = \frac{V cos\gamma cos\psi}{r} \tag{3}$$

$$\dot{V} = -D - \frac{sin\gamma}{r^2} + {\omega_e}^2 r cos\phi\,(sin\gamma cos\phi - cos\gamma sin\phi cos\psi) \tag{4}$$

$$\dot{\gamma} = \frac{1}{V}\left[Lcos\sigma + \left(V^2 - \frac{1}{r}\right)\left(\frac{cos\gamma}{r}\right) + 2\omega_e V cos\phi sin\psi + \omega_e^2 r cos\phi\,(cos\gamma cos\phi - sin\gamma cos\psi sin\phi)\right] \tag{5}$$

$$\dot{\psi} = \frac{1}{V}\left[L\frac{sin\sigma}{cos\gamma} + \frac{V^2}{r}cos\gamma sin\psi tan\theta - 2\omega_e V(tan\gamma cos\psi cos\phi - sin\phi) + \frac{\omega_e^2}{cos\gamma}sin\psi sin\phi cos\phi\right] \tag{6}$$

DOI: 10.13009/EUCASS2017-545

here r is the geocentric radius from center of the Earth to the reentry vehicle normalized by the radius of Earth $R_0 = 6378\ (km)$. ω_e is the Earth angular velocity normalized by $\sqrt{(g_0/R_0)}$. D and L are the dimensionless aerodynamic drag and lift accelerations in terms of g's where as ρ is the atmospheric density such as

$$D = \frac{\rho (V_c V)^2 S_{ref} C_D}{2mg_0} \tag{7}$$

$$L = \frac{\rho (V_c V)^2 S_{ref} C_L}{2mg_0} \tag{8}$$

$$\rho = \rho_s e^{-r-R_0/\beta} \tag{9}$$

here ρ_s is the atmospheric density at sea level and β is the atmospheric height with even density. Mass m in kg, surface area S_{ref} in m^2 along with the 2-D look up tables for computing lift C_L and drag C_D coefficients of CAV as function of angle of attack and mach number are mentioned in Phillips.[14] The longitude and latitude are θ and ϕ respectively. The Earth relative velocity V is normalized by $V_c = \sqrt{(g_0 R_0)}$ with $g_0 = 9.81 m/s^2$. Flight path angle is expressed by using γ, where as ψ is the velocity azimuth angle, positive in clockwise direction from the North. The variation of above model is w.r.t the dimensionless time $\tau = t\sqrt{(R_0/g_0)}$. The bank angle σ shall be used as the control signal which is to be optimized as σ_b in bézier time domain t_b. Interpolation is used to extract the control signal σ w.r.t the actual flight time t, expressed here as the dimensionless variable τ. The detailed formulation for computing σ_b is given in Sec. 4.3.

2.2 Genetic Algorithm

A brief introduction of classical genetic algorithm is explained in this section. The population in genetic algorithm consists of design variables initially selected at random from the design range. An individual or single design parameter is encoded as a chromosome in bits of predefined length. Characteristics of genes for each design variable is associated with the subsets of bits in the form of chromosome strings, which gives physical meaning to the solution. Fitness function is used to rank the individual chromosome. High ranked individuals shall be used to produce next generation of better fitness values. Chromosomes of randomly chosen pairs out of breeding pool are crossed over to fill the new population.
Mutation or bit flip is sometimes used to change the parents characteristics into their child, in order to maintain diversity and to avoid early solution convergence. Evolution algorithm continues until following condition achieved, 1- Fitness function J_{min} saturates before predefined stall generations. 2- Generation stalls N_{max}. The detailed pseudo code for classical genetic algorithm is explained through Algorithm 1.

Solution guess encoding to define chromosome;
Data: Initialize number of chromosomes, stall generations, mutation and crossover rates
Evaluate initial population according to fitness criteria;
Result: Chromosome population decoding to provide best solution
while N_{max} *or* J_{min} **do**
    Select chromosome for next population using Roulette Wheel selection;
    Crossover pairs of parents to generate two offsprings;
    Mutate the resulting offsprings;
    Evaluation of fitness value of each chromosome through objective function;
end

Algorithm 1: Classical Genetic Algorithm

2.3 Rational Bézier Curve

Bézier curve is a parametric curve, which is a function of control points P and bézier parameter w. It is used in graphical design applications. Rational bézier curves is an extension of bézier method which assigns weight μ_i to each control point P to provide closer approximation to scattered shapes. The expression for rational bézier curve is given as:

DOI: 10.13009/EUCASS2017-545

$$B(w) = \frac{\sum_{i=0}^{n} b_{i,n}(w) P_i \mu_i}{\sum_{i=0}^{n} b_{i,n}(w) \mu_i} \tag{10}$$

where the polynomials

$$b_{i,n}(w) = \binom{n}{i} w^i (1-w)^{n-i}, i = 0, 1, ..., n \tag{11}$$

are known as Bernstein[12] basis polynomials of degree n. P_i are the number of control points for rational bézier curve. Bézier parameter w generates the trajectory line, starting from first control point P_0 to the last control point P_n, and is varied from $0 \leq w \leq 1$.
In our proposed method, control points $P_i = [\phi_i, \theta_i, r_i]^T$ are defined in terms of latitude ϕ, longitude θ and radial distance r taken from the center of the Earth. The control points with the corresponding weight factor in Eq. 10 are represented as $[\mu_i b_i^T \mu_i]^T$, $i = 0, 1....n$. Here weight coefficients are denoted as μ_i and should be greater than zero i-e $\mu_0, \mu_n \geq 0$. If all the weights μ_i assigned to n control points are equal to 1, then Eq. 10 will reduced to irrational bézier curve.
De Casteljau's algorithm a recursive method has been used to evaluate polynomials expressed in Bernstein form of bézier curve and is expressed as:

$$B(w) = \frac{\sum_{i=0}^{n-k} \mu_i^k b_i^k P_{i,n-k}(w)}{\sum_{i=0}^{n-k} \mu_i^k P_{i,n-k}(w)} = ... = b_0^n \tag{12}$$

The intermediate weight factor and control points are expressed as

$$\mu_i^k = \begin{cases} \mu_i, & k = 0. \\ (1-w)\mu_i^{k-1} + w\mu_{i+1}^{k-1}, & k = 1, 2, ..., n; i = 0, 1, ..., n-k. \end{cases} \tag{13}$$

$$b_i^k = \begin{cases} b_i, & k = 0. \\ (1-w)\frac{\mu_i^{k-1}}{\mu_i^k} b_i^{k-1} + w\frac{\mu_{i+1}^{k-1}}{\mu_i^k} b_{i+1}^{k-1}, & k = 1, 2, ..., n; i = 0, 1, ..., n-k. \end{cases} \tag{14}$$

The k represents the recursive series, where each recursive derivative of the rational bézier curve will reduce one control point. In order to compute the derivative of rational bézier curve given by Eq. 12, let the numerator and denominator of this equation are represented as

$$B^*(w) = \sum_{i=0}^{n} \mu_i b_i P_{i,n}(w) \tag{15}$$

$$\mu(w) = \sum_{i=0}^{n} \mu_i P_{i,n}(w) \tag{16}$$

The first and second order derivative of Eq. 12 is computed as

$$B'(w) = \frac{d}{dw} B(w) = \frac{1}{\mu(w)} \left[B^{*\prime}(w) - \mu'(w) B(w) \right] \tag{17}$$

$$B''(w) = \frac{d^2}{dw^2} B(w) = \frac{1}{\mu(w)} \left[B^{*}(w) - 2\mu'(w) B'(w) - \mu''(w) B(w) \right] \tag{18}$$

DOI: 10.13009/EUCASS2017-545

The convergence time required by genetic algorithm is directly proportion to the number of design variables i-e total number of control points. The computation time for trajectory optimization though genetic algorithm is reduced by using rational bézier curves. With different values of weight μ_i assigned to each control point, different shapes of bézier trajectories against same number of control points is possible. Thus, the application of rational bézier curve in our proposed research reduces the total number of design variables required to achieve optimized trajectory, which could have been larger in case of irrational bézier curves, illustrated through Fig. 1.

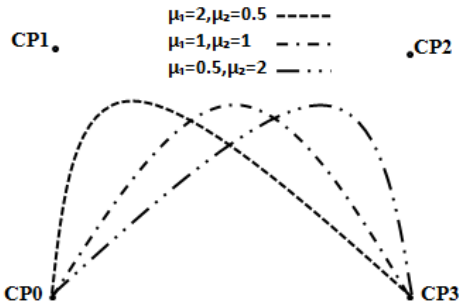

Figure 1: Change in rational bézier curves due to μ_i

3. Entry Trajectory Constraints

Common aero vehicle entry trajectory path constraints are listed below

$$\dot{Q} \leq \dot{Q_{max}} \tag{19}$$
$$q \leq q_{max} \tag{20}$$
$$|Lcos\alpha + Dsin\alpha| \leq n_{Zmax} \tag{21}$$

Trajectory path constraints includes allowable rate rates given by Eq. 19, where maximum limit of $\dot{Q} = k\sqrt{\rho}V^{3.15}$ is defined against the constant value of $k = 5.21 \times 10^{-8}$. Heat rates on the surface of CAV increases due to air frictions at hypersonic speeds. Thus to avoid surface deformation, heating rates must be controlled. Higher dynamic pressures at hypersonic velocities generates excessive normal force, even at small angle of attacks. Normal force is required to get maximum range but should be controlled to avoid stall conditions. Hence, the dynamic pressure $q = \rho V^2/2$ is treated as a path constraint and is defined by Eq. 20. Total aerodynamic load is constrained in the normal direction using Eq. 21. This n_{max} is the maximum allowable g and is a function of structural limit and control power of CAV.
Equilibrium glide condition (EGC) is introduced by Zhang et al[21] to reduce phugoid oscillations in entry trajectory altitude profile. EGC ensures bank angle margins such that $\sigma \geq \sigma_{EQ}$ through equation

$$\left[1/r - V^2\right](1/r) - Lcos(\sigma_{EQ}) \leq 0$$

In our proposed methodology, this constraints is inherently handled by providing co-altitudes to all the control points as an initial guess for the genetic algorithm. Since, the initial population guess influences the genetic algorithm solution convergence, hence final solution in terms of optimized control points has reduced phugoids in altitude profile. The reduction in the number of altitude phugoids will optimized CAV trajectory flight time as shown in the Sec. 5.
The entry trajectory of CAV must have correct terminal conditions as provided by terminal area attack management ($TAAM$) guidance system to ensure right approach towards the target point. Thus the terminal constraints for the entry trajectory, in terms of the requirements laid down by TAAM are listed as

$$\delta V_f \leq \delta V_{TAAM} \tag{22}$$
$$\delta \gamma_f \leq \delta \gamma_{TAAM} \tag{23}$$
$$\delta \psi_f \leq \delta \psi_{TAAM} \tag{24}$$
$$lla_f = lla_{TAAM} \tag{25}$$

DOI: 10.13009/EUCASS2017-545

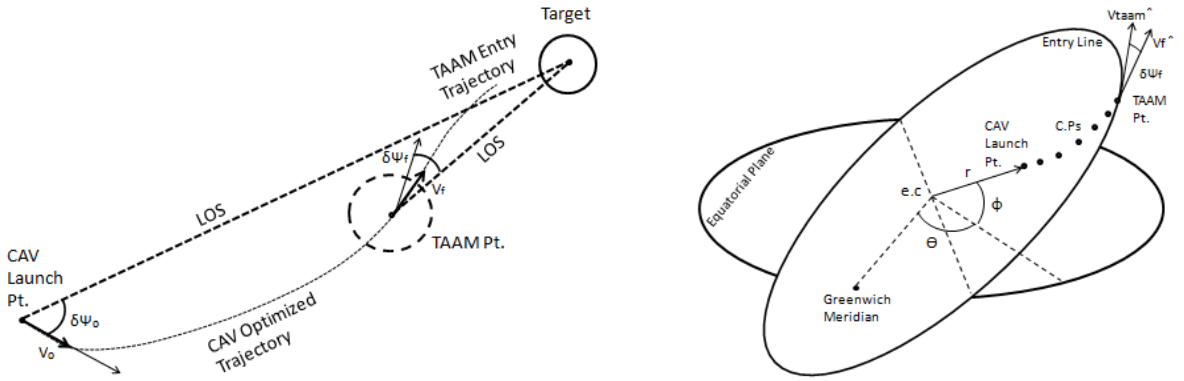

(a) Heading error along entry trajectory

(b) CAV entry geometry

Figure 2: Common aero vehicle heading error (a) along entry trajectory (b)

where $\delta V_f = V_{TAAM} - V_f$, and δV_{TAAM} is the allowable error bound for terminal velocity at the end of entry trajectory. Similarly lla_f is the last control point for rational bézier curve and should match with the initial value of lla_{TAAM} at the commencement of TAAM guidance phase. For TAAM phase, the required flight path error $\delta\gamma_f = \gamma_{TAAM} - \gamma_f$ and azimuth error $\delta\psi_f = \psi_{TAAM} - \psi_f$ should be less than $\delta\gamma_{TAAM}$ and $\delta\psi_{TAAM}$ respectively, see Fig. 2a. These constraints are set as the hard constraints, and must be satisfied to ensure correct TAAM guidance phase as shown in Fig. 2b.

4. Trajectory Optimization for CAV

Re-entry trajectory for CAV satisfying all constraints has been achieved using rational bézier curve aided with genetic algorithm. Differential calculus is used to transform the CAV dynamic model given by Eqs. 1-6, from time domain into the bézier. The bézier model of CAV is then used by the genetic algorithm to compute fitness function. Fitness function for genetic algorithm consists of trajectory constraints defined by Eqs. 19-24. The terminal point constraint of Eq. 25 is naturally satisfied as a last point of bézier trajectory. Rational bézier curve is used to compute guidance command in terms of bank angle σ_b in bézier domain. Finally, the guidance command σ in flight time t, should be interpolated form σ_b defined in bézier time t_b. This bank angle σ can then be used as a control command for CAV dynamic model represented by Eqs. 1-6. Following are the detailed formulations required to achieve aforementioned objectives.

4.1 Computations of the Control Points

The design variables for genetic algorithm are defined in terms of the control points positions *(excluding first and the last control point)*, along with the weight factor μ associated with all the control points *(including first and the last control point)*.

$$\Phi = [R_1, \theta_2, ..., \theta_{n-1}, r_2, ...r_n, \mu_0, ...\mu_n]^T \tag{26}$$

here R_1 is the initial ground range between first and the second control point. Initial bearing ψ_0 and ground range R_1 can be used to compute latitude ϕ_1 and longitude θ_1 associated with the second control. The radial distance r_1 assign to the second control point can be computed using initial flight path angle γ_0, radial distance r_0 and ground range R_1 such as $r_1 = r_0 + R_1 \tan\gamma_0$. Latitudes assign to the middles control points is evenly divided from the second point latitude ϕ_1 to the last point latitude ϕ_n using relation

$$\phi_i = \frac{\phi_n - \phi_1}{n-1}(i-1), i = 2, ...n-1 \tag{27}$$

The genetic algorithm design variables mentioned in Eq. 26 provide longitude θ_i and radial distance r_i associated with the middle control points between second $P_1 = [\phi_1, \theta_1, r_1]$ and the last control point P_n. First control point P_0 is the initial entry trajectory point and the last control point P_n is the required terminal point lla_{TAAM} given by Eq. 25. Hence, the array of geodetic control points starting from first point P_0 to last point P_n is given by

DOI: 10.13009/EUCASS2017-545

$$P_i = [\phi_i, \theta_i, r_i]^T, i = 0, ...n \tag{28}$$

4.2 CAV Dynamic Model in Bézier Domain

Rational bézier curve is used to approximate the trajectory using geodetic control points P_i and the corresponding weight factor μ_i where w is the bézier parameter varies from $0 \leq w \leq 1$ and $i = 0, ...n$. State variables in bézier domain are expressed as

$$x_b = [t_b \; r_b(P,w) \; \theta_b(P,w) \; \phi_b(P,w) \; V_b \; \gamma_b \; \psi_b]^T \tag{29}$$

here $r_b(P,w)$, $\theta_b(P,w)$, and $\phi_b(P,w)$ are the direct function of control points P_i and weight factor μ_i where as, t_b, V_b, γ_b, and ψ_b are indirect function of control points and weight factor computed below. t_b is the bézier time with first and second order derivative of bézier curve as a function of P and w using Eq. 17 and Eq. 18 are computed as

$$B'(P,w) = [\phi'(P,w) \; \theta'(P,w) \; r'(P,w)]^T \tag{30}$$
$$B''(P,w) = [\phi''(P,w) \; \theta''(P,w) \; r''(P,w)]^T \tag{31}$$

Elements of $B'(P,w)$ and $B''(P,w)$ can be computed using De Casteljau's algorithm mentioned above. State variables ψ_b and γ_b can be expressed in bézier domain using equations Eq. 2 and Eq. 6

$$\psi_b = \tan^{-1}\left[\frac{cos\phi(P,w) \; \theta'(P,w)}{\phi'(P,w)}\right] \tag{32}$$
$$\gamma_b = \tan^{-1}\left[\frac{cos\psi_b \; r'(P,w)}{\phi'(P,w) \; r(P,w)}\right] \tag{33}$$

Derivative of above equations gives

$$\dot{\psi_b} = \left[\frac{((\phi'(P,w)\theta'(P,w)cos\phi(P,w)) - (\phi'(P,w)^2 sin\phi(P,w)\theta'(P,w)))- (\phi''(P,w)cos\phi(P,w)\theta''(P,w))}{\phi'(P,w)^2}\right] cos\psi_b^2 \tag{34}$$

$$\dot{\gamma_b} = \left[\frac{((cos(\psi_b)r''(P,w)\phi'(P,w)r(P,w)) - (\phi'(P,w)r(P,w)sin(\psi_b)\dot{\psi}_b r'(P,w)))- (((cos(\psi_b)r'(P,w)^2\phi'(P,w)) + (cos(\psi_b)r'(P,w)\phi''(P,w)r(P,w)))}{(\phi'(P,w)r(P,w))^2}\right] cos(\gamma_b)^2 \tag{35}$$

Differential calculus used to change the dependence of state variables from time domain (d/dt) to bézier domain (d/dw) is used as

$$\frac{dx}{dt} = \frac{dx}{dw} \times \frac{dw}{dt} \tag{36}$$

where the change in bézier state variables x_b' w.r.t bézier parameter w is

$$x_b' = \frac{dx}{dw} = \frac{dx}{dt} \times \frac{dt}{dw} \tag{37}$$

using Eq. 1 the differential equation for bézier time t_b can be expressed as

DOI: 10.13009/EUCASS2017-545

$$t'_b = \frac{dt}{dw} = \frac{r'(P,w)}{(V_b \sin\gamma_b)} \tag{38}$$

Bézier time derivative calculated from above Eq. 38 is used to update the velocity variable w.r.t the bézier parameter w. Hence, using Eq. 4 and Eq. 38 the derivative of velocity V'_b is formulated as

$$V'_b = \left[-D - \frac{sin(\gamma_b)}{r(P,w)^2} + {\omega_e}^2 r(P,w) cos(\phi(P,w))\,(sin(\gamma_b)cos(\phi(p,w)) - cos(\gamma_b)sin(\phi(P,w))cos(\psi_b))\right] \times \left[\frac{r'(P,w)}{(V_b \sin\gamma_b)}\right] \tag{39}$$

It is pertinent to summarize here that expressions used to compute the derivatives x'_b of all the states mentioned in Eq. 29 have been formulated, where Eq. 30 and Eq. 31 computes the derivative of r_b, θ_b and ϕ_b as a function of control points P and bézier parameter w. Eq. 34 and Eq. 35 expressed the derivative of state variable γ_b and ψ_b. The change in the state variables of V_b and t_b can be estimated by integrating equations Eq. 38 and Eq. 39 using bézier step size of δw. Thus the dynamic model of CAV in bézier domain is represented as

$$x'_b = [t'_b\ r'_b(P,w)\ \theta'_b(P,w)\ \phi'_b(P,w)\ V'_b\ \gamma'_b\ \psi'_b]^T \tag{40}$$

4.3 Trajectory Guidance Commands

The guidance commands for entry trajectory of CAV composed of longitudinal guidance α and lateral guidance commands σ with later is the main part. In order to control the high heat flow in the early stage of the entry, rapid decrease in flight velocity with high angle of attack plays a pivotal role. The reference profile of angle of attack α w.r.t the mach number mentioned in Fig. 3 has been taken from the shuttle flight experience in Harpold et al.[10] This α profile w.r.t mach number indicates that requirement of low angle of attack α at the terminal phase of the entry guidance, it also improve lateral maneuver ability in terms of decreasing phugoid oscillation and increasing flight range. Hence, the variation of attack angle balanced the heat flow requirement and lateral maneuver ability at the start and terminal phase of the entry guidance respectively.

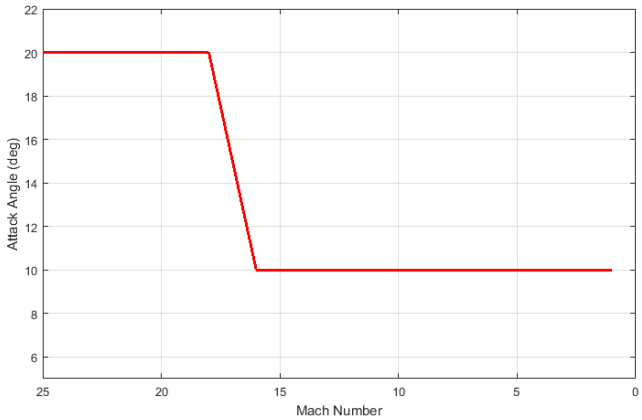

Figure 3: Reference profile of angle of attack

The bank angle σ is the lateral guidance command which is computed analytically by using relation

$$\frac{d\gamma}{dw} = \frac{d\gamma}{dt} \times \frac{dt}{dw} \tag{41}$$

after substituting the expressions for $d\gamma dw$, $d\gamma dt$ and $dtdw$ from the equations Eq. 35, Eq. 5 and Eq. 38 respectively, bank angle command σ_b in bézier domain is formulated as

DOI: 10.13009/EUCASS2017-545

$$\sigma_b = cos^{-1}\left[\frac{\left[\begin{array}{l}\frac{\gamma_b' V_b^2 \sin\gamma_b}{r'(P,w)} - \left(V_b^2 - \frac{1}{r(P,w)}\right)\left(\frac{cos\gamma_b}{r(P,w)}\right) - 2\omega_e V_b cos(\phi(P,w))sin\psi_b - \\ \quad \omega_e^2 r(P,w)cos(\phi(P,w))\left(cos\gamma_b cos(\phi(P,w)) - sin\gamma_b cos\psi_b sin(\phi(P,w))\right)\end{array}\right]}{L}\right] \tag{42}$$

The Sec. 5 includes the 3-DoF optimized trajectory of CAV in actual flight time t, computed from the guidance command σ. The lateral guidance command σ in time domain t can be linearly interpolated from the σ_b in bézier time domain t_b

$$\sigma = \sigma_{b_1} + (\sigma_{b_2} - \sigma_{b_1})\frac{t - t_{b_1}}{t_{b_2} - t_{b_1}} \tag{43}$$

here (t_{b_1}, σ_{b_1}) and (t_{b_2}, σ_{b_2}) represents the two points separated by δw.

4.4 Fitness Function for Genetic Algorithm

The control point optimization through genetic algorithm depends upon the minimization of the following fitness function J

$$J = \int_0^1 t_b(w)dw + L_f \tag{44}$$

where L_f for k number of constraints is defined as

$$L_f = p\sum_{i=1}^{k} G_k, G_k = \max(0, g_k) \tag{45}$$

here p is the penalty value for fitness function and g_k is a function of path constraints defined in Eqs. 19-21 and terminal error constraints from Eqs. 22-24.

$$\begin{aligned} g_1 &= \frac{inf\ n_Z}{n_{Zmin}} - 1 \leq 0, \quad g_2 = \frac{sup\ n_Z}{n_{Zmax}} - 1 \leq 0 \\ g_3 &= \frac{sup\ q}{q_{max}} - 1 \leq 0, \quad g_4 = \frac{sup\ Q}{Q_{max}} - 1 \leq 0 \\ g_5 &= \frac{\delta V_f}{\delta V_{TAAM}} - 1 \leq 0, \ g_6 = \frac{\delta\gamma_f}{\delta\gamma_{TAAM}} - 1 \leq 0 \\ g_7 &= \frac{\delta\psi_f}{\delta\psi_{TAAM}} - 1 \leq 0 \end{aligned}$$

where

$$\begin{aligned} inf\ n_Z &= \min\left(n_Z(w_i) \mid w_i \in [0,1], i = 1, 2...m\right) \\ sup\ n_Z &= \max\left(n_Z(w_i) \mid w_i \in [0,1], i = 1, 2...m\right) \\ sup\ q &= \max\left(q(w_i) \mid w_i \in [0,1], i = 1, 2...m\right) \\ sup\ Q &= \max\left(Q(w_i) \mid w_i \in [0,1], i = 1, 2...m\right) \end{aligned} \tag{46}$$

In the above equation $m = w/\delta w$ is the total number of steps for bézier parameter w as it goes from 0 *to* 1. The terminal point constraint of $lla_{TAAM} = [\phi_f\ \theta_f\ r_f]^T$ is naturally satisfied by selecting last control point as

$$P_n = lla_{TAAM} \tag{47}$$

DOI: 10.13009/EUCASS2017-545

5. Simulation Results

The CAV trajectory optimizations has been achieved using 3-DoF simulation based on the dynamic model mentioned in Eq. 1 to Eq. 6 using bank angle control input $\sigma(t)$. This control signal σ w.r.t flight time t. Validation of the proposed method has been achieved using state-of-art GPOPS-II general purpose matlab software. Boundary conditions used in this simulation are mentioned in Tab. 1.

Table 1: Boundary Condition for CAV 3-DoF Simulation

	Initial Value$_0$	**Final Value$_f$**	**Unit**
Latitude(ϕ)	0	34.5	deg
Longitude(θ)	0	75.5	deg
Altitude(a^*)	121920	24518	m
Velocity(V)	7802	$\delta V_f \leq \delta V_{TAAM}$	m/s
Flight Path Angle(γ)	-2.4	$\delta\gamma_f \leq \delta\gamma_{TAAM}$	deg
Azimuth Angle(ψ)	90	$\delta\psi_f \leq \delta\psi_{TAAM}$	deg

*Radius distance $r = a + R_0$

Optimized design variables Φ computed by genetic algorithm were shown in Tab. 2. The elements of Φ consists of initial ground range, control points values in terms of longitude and radial distance along with the weight associated with each control point, including weight factor for first and the last control point. Necessary conversions used to compute bézier control points P_i from design variables Φ is mentioned in Sec. 4.1.

Table 2: Optimized design variables

	R_1/km	$\theta_2(rad)$	$\theta_3(rad)$	$\theta_4(rad)$	$\theta_5(rad)$	r_2/km	r_3/km	r_4/km	r_5/km
Φ^*	112.98	0.54	0.48	0.29	0.67	42.29	96.80	53.00	104.37

* Optimized control points geodetic positions

Table 3: Optimized design variables

	μ_0	μ_1	μ_2	μ_3	μ_4	μ_5	μ_6
Φ^b	14.41	19.00	12.40	1.40	18.17	5.29	10.46

^{b} Optimized control points weight factor

TAAM error bounds against the boundary conditions mentioned in Tab. 1 are taken from Zuojun et al.[15] The acceptable error bounds for TAAM entry trajectory must be satisfied in order to approach towards the target point. The reference values of TAAM error bonds serves as the terminal constraints for CAV optimal trajectory. Tab. 4 shows the trajectory path and terminal TAAM entry constraints against the geometric bounds of Tab. 1.

Table 4: Trajectory Path and Terminal Constraints

	$\mathbf{n_{Zmax}}$	$\mathbf{q_{max}}$	$\dot{\mathbf{Q}}_{\mathbf{max}}$	$\delta\mathbf{lla_{TAAM}}$	$\delta\mathbf{V_{TAAM}}$	$\delta\gamma_{\mathbf{TAAM}}$	$\delta\psi_{\mathbf{TAAM}}$
Path Constraints	$5\ g's$	$162800\ N/m^2$	$70\ BTU/ft^2/sec$	-	-	-	-
Terminal Constraints	-	-	-	$0, 0, 0\ m$	$300\ m/sec$	$5\ deg$	$10\ deg$

Since the bézier curve touches only first and last control point thus, the trajectory terminal constraints in terms of ϕ_f, θ_f and r_f are always satisfied. The optimized three dimensional trajectory plot is shown in the Fig. 4a, which is constructed from the total number of $n = 7$ control points. Using Sec. 4.1, optimized five points from final design variables returned from genetic algorithm at 2^{nd} generation, along with the optimized weight factor for all seven control points are listed in Tab. 5.

DOI: 10.13009/EUCASS2017-545

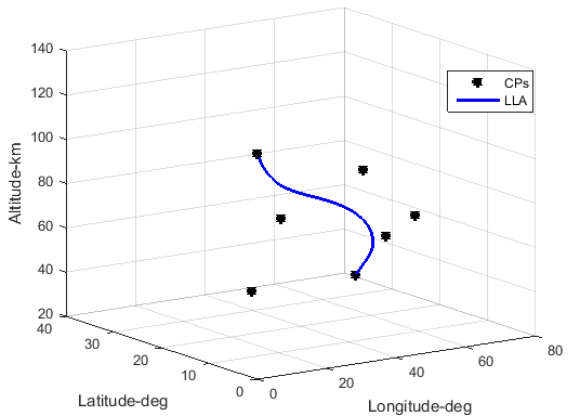

(a) 3D trajectory from optimized CPs

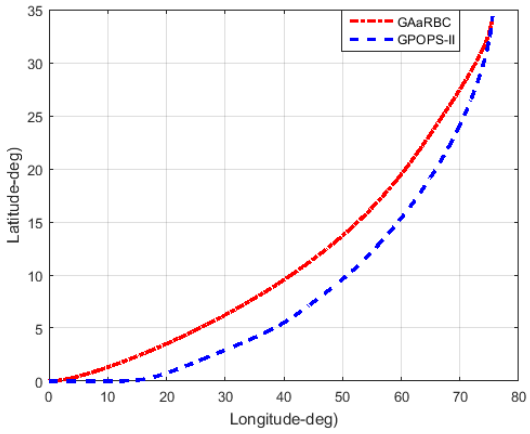

(b) 2D GAaRBC trajectory compared with GPOPS-II

Figure 4: GAaRBC optimized trajectory

Table 5: Optimized control points and weight factors

	$\mathbf{CP_0}$	$\mathbf{CP_1}$	$\mathbf{CP_2}$	$\mathbf{CP_3}$	$\mathbf{CP_4}$	$\mathbf{CP_5}$	$\mathbf{CP_6}$
Latitude (deg)	ϕ_0	4.079	6.872	13.745	20.617	27.490	ϕ_{TAAM}
Longitude (deg)	θ_0	6.677	39.779	64.117	26.677	74.612	θ_{TAAM}
Altitude* (km)	a_0	90.797	100.172	68.888	38.746	47.282	a_{TAAM}
Weight Factor	9.985	13.882	9.923	11.473	13.487	12.124	11.254

*Radius distance $r = a + R_0$

The verification of trajectory optimization using proposed method of genetic algorithm aided with rational bézier curve (GAaRBC) has been achieved by modeling comparative simulations with state of the art optimization algorithm GPOPS-II. The boundary conditions in Tab. 1 and trajectory constraints in Tab. 4 has been kept same for both the simulations. It can be concluded that GAaRBC reduces the phugoids in altitude trajectory, which gives the optimal flight time as compared with GPOPS-II simulation, as shown in Fig. 5a. The dynamic pressure constraint necessary to maintain the required lift in Fig. 5b is less than the limit specified by Tab. 4.

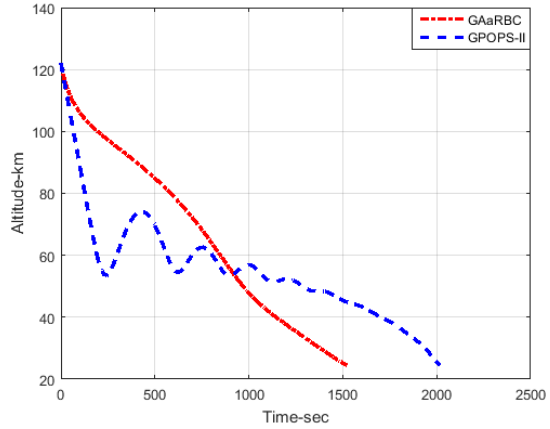

(a) GAaRBC altitude compared with GPOPS-II

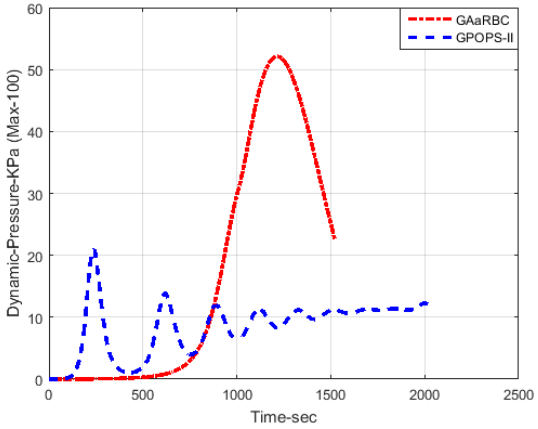

(b) GAaRBC dynamic pressure compared with GPOPS-II

Figure 5: GAaRBC altitude (a) and dynamic pressure (b) compared with GPOPS-II

GAaRBC bank angle command σ compared with GPOPS-II w.r.t flight time t is shown in Fig. 6a. Presently there is no limit on the control command σ, thus GAaRBC control command is higher than GPOPS-II. Secondly, bank angle turn generated through GAaRBC is acceptable until it is less than 90 degrees, and does not violate path constraint of

DOI: 10.13009/EUCASS2017-545

normal loading n_{Zmax} as shown in Fig. 6b.

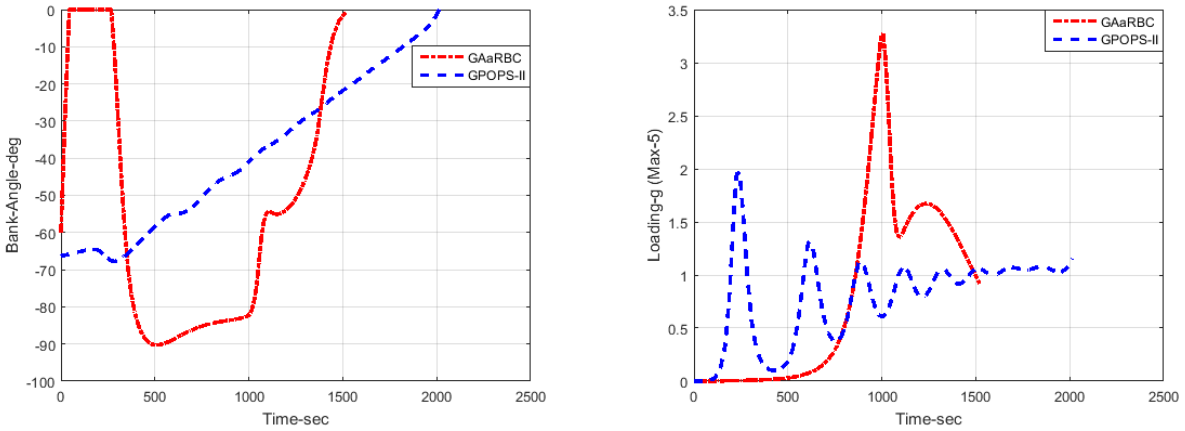

(a) GAaRBC bank angle compared with GPOPS-II

(b) GAaRBC normal loading compared with GPOPS-II

Figure 6: GAaRBC bank angle (a) and normal loading (b) compared with GPOPS-II

The path constraint of heating rate as compared with GPOPS-II is shown in the Fig. 7a. The heating rate constraint has been violated in total 11% of the total flight time in GAaRBC. The altitude and speed comparison plots in Fig. 5a and Fig. 7b explains this phenomena i-e in order to reduce phugoid oscillations to achieve minimum flight time, the initial launch velocity is maintained under the effect of gravity during constant decrease in altitude profile. Later, low altitude density and reduced altitude descent slope, reduces trajectory velocity to the required terminal value of V_{TAAM}.

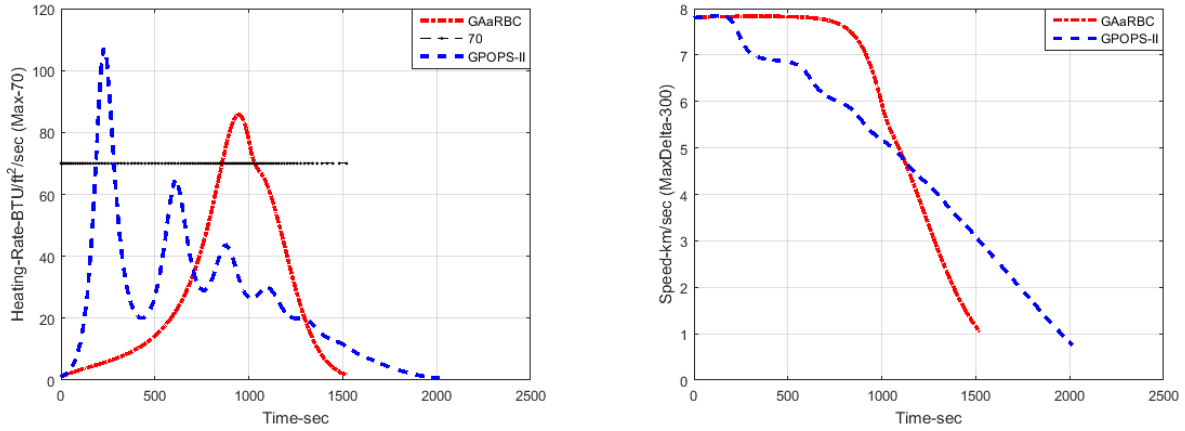

(a) GAaRBC heating rate compared with GPOPS-II

(b) GAaRBC velocity compared with GPOPS-II

Figure 7: GAaRBC heating rate (a) and velocity (b) compared with GPOPS-II

Table 6: Evaluation of terminal trajectory constraints

	$\mathbf{V_f}$	$\gamma_\mathbf{f}$	$\psi_\mathbf{f}$	V_{TAAM}	$\gamma_\mathbf{TAAM}$	$\psi_\mathbf{TAAM}$	$\lvert\delta\mathbf{V_{TAAM}}\rvert$	$\lvert\delta\gamma_\mathbf{TAAM}\rvert$	$\lvert\delta\psi_\mathbf{TAAM}\rvert$	t_f
GAaRBC	1044m/s	$-1.7°$	$6.3°$	800m/s	$-5°$	$10°$	244m/s	$3°$	$3.7°$	1520s
GPOPS-II	762m/s	$-5.0°$	$7.5°$	800m/s	$-5°$	$10°$	38m/s	$0°$	$2.5°$	2014s

Terminal values of flight path angle γ_f, heading angle ψ_f and velocity V_f as required by TAAM initial descent phase are assumed to be our terminal constraints. The acceptable error bounds to achieve TAAM phase, are given by Tab. 4. The evaluation of trajectory terminal constraints along with the final time t_f using GAaRBC and GPOPS-II are shown in Tab. 6. It can be concluded that δ_{TAAM} achieved by GOPOS-II are better than GAaRBC but, firstly δ_{TAAM} computed using GAaRBC are with in the tolerance as provided by Tab. 4, secondly significant improvement in terms of terminal

DOI: 10.13009/EUCASS2017-545

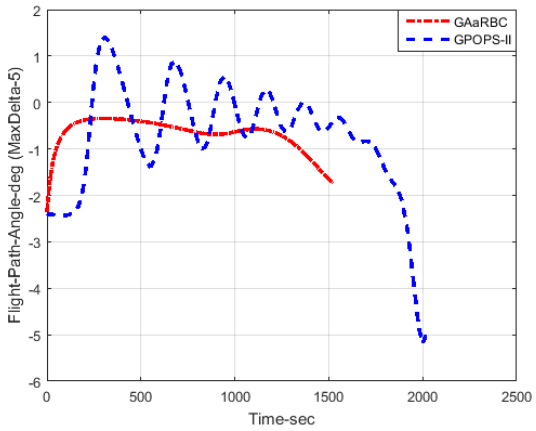

(a) GAaRBC flight path angle compared with GPOPS-II

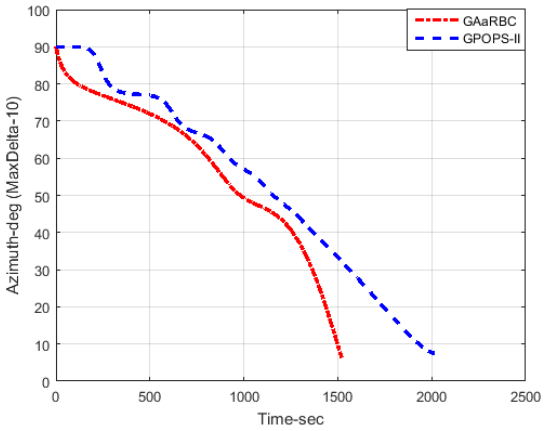

(b) GAaRBC heading compared with GPOPS-II

Figure 8: GAaRBC trajectory angles compared with GPOPS-II

time has been achieved through GAaRBC while hitting the same terminal point of lla_{TAAM}. The variation of flight path angle γ and heading angle ψ in comparison with GPOPS-II are shown in the Fig. 8a and Fig. 8b respectively. Fig. 9 shows ground trajectories of CAV using GAaRBC, at different initial conditions against common trajectory constraints. Tab. 7 compare terminal value of each case against the required constraints to evaluate the performance of GAaRBC in a complete dynamic environment. All the cases are with in the tolerance as specified by TAAM guidance system.

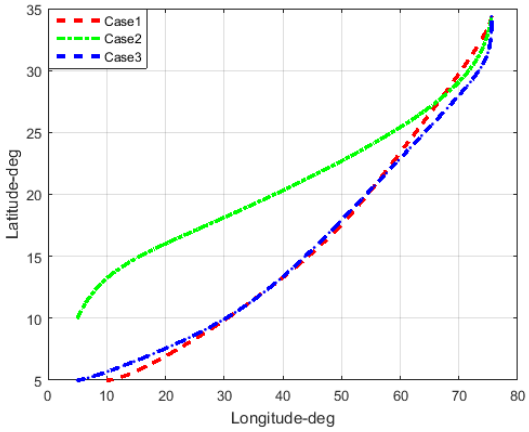

Figure 9: 2D GAaRBC trajectories at different initial conditions

Table 7: Evaluation at different initial conditions

	$\mathbf{V_f}$	$\gamma_\mathbf{f}$	$\psi_\mathbf{f}$	V_{TAAM}	$\gamma_\mathbf{TAAM}$	$\psi_\mathbf{TAAM}$	$\lvert\delta\mathbf{V_{TAAM}}\rvert$	$\lvert\delta\gamma_\mathbf{TAAM}\rvert$	$\lvert\delta\psi_\mathbf{TAAM}\rvert$	t_f
Case1	956m/s	$-1.5°$	$9.3°$	800m/s	$-5°$	$10°$	156m/s	$3.5°$	$0.7°$	1218s
Case2	920m/s	$-2.0°$	$8.5°$	800m/s	$-5°$	$10°$	120m/s	$3°$	$1.5°$	1316s
Case3	905m/s	$-2.5°$	$2.3°$	800m/s	$-5°$	$10°$	105m/s	$2.5°$	$7.7°$	1845s

6. Conclusions

Optimal trajectory of common aero vehicle based on the optimized control points is efficient in terms of flight time as compared with the GPOPS-II. The application of rational bézier reduces number of design variables, required to be optimized by genetic algorithm. Genetic algorithm fitness function handles path constraints and terminal constraints.

DOI: 10.13009/EUCASS2017-545

Terminal TAAM entry point is naturally satisfied as bézier curve last control point. The bank angle command σ interpolated form σ_b at flight time t, is used to compute CAV optimized trajectory. Bézier parameter at $w = 0$ gives initial states where as terminal values can be analyzed by setting w=1. Thus different values of w allow us to handle multiple constraints at different trajectories points.
The idea of using control points in design space reduces the number of design variables and could save the computational time. Future endeavours can use this novel idea to implement real time on-board optimal guidance against the dynamic targets.

7. Acknowledgments

This research was supported by the National Science Foundation of China under Grants 61502391.

References

[1] K. Clarke A. Rao. Performance optimization of a maneuvering re-entry vehicle using a legendre pseudospectral method. (*AIAA*) *Atmospheric Flight Mechanics Conference and Exhibit*, 2002.

[2] John T. Betts. Survey of numerical methods for trajectory optimization. *Journal of Guidance Control and Dynamics*, 21(2):193–207, 1998.

[3] G. Tang E. Yong and L. Chen. Three-dimensional optimal trajectory for global range of cav. *1st International Symposium on Systems and Control in Aerospace and Astronautics*, pages 1396–1400, 2006.

[4] I.M. Ross F. Fahroo. Direct trajectory optimization by a chebyshev pseudospectral method. (*IEEE*) *Proceedings of 2000 American Control Conference*, 6:3860–3864, 2000.

[5] R. I. Michael F. Fariba. Costate estimation by a legendre pseudospectral method. *Journal of Guidance Control and Dynamics*, 24(2):270–277, 2001.

[6] M.-S. Kim G. E. Farin, J. Hoschek. *Handbook of Computer Aided Geometric Design*. Elsevier, 2002.

[7] R. George. The common aero vehicle - space delivery system of the future. (*AIAA*) *Space Technology Conference and Exposition*, 1999.

[8] R. George and H. John. Striking from space - the future of space force applications. (*AIAA*) *Defense and Civil Space Programs Conference and Exhibit*, 1998.

[9] S. Mathavaraj H. Omkar and P. Radhakant. Energy based suboptimal reentry guidance of a reusable launch vehicle using model predictive static programming. (*AIAA*) *Guidance, Navigation, and Control Conference*, 2010.

[10] J. C. Harpold. Shuttle entry guidance. *Journal of Astronautical Sciences*, 37:239–268, 2015.

[11] R. Zhou J. Zhao and X. Jin. Reentry trajectory optimization based on a multistage pseudospectral method. *The Scientific World Journal*, pages 1–13, 2014.

[12] E. Kreyszig. Bernstein polynomials and numerical integration. *International Journal for Numerical Methods in Engineering*, 14(2):292–295, 1979.

[13] A. V. Rao M. Patterson. Gpops-ii. *ACM Transactions on Mathematical Software*, 41(1):1–37, 2014.

[14] T. H. Phillips. *A Common Aero Vehicle (CAV) Model, Description, and Employment Guide*. Schafer Corporation, 2003.

[15] P. Lu S. Zuojun. On-board generation of three-dimensional constrained entry trajectories. (*AIAA*) *Guidance, Navigation and Control Conference and Exhibit*, 2002.

[16] D.K. Sachdev. Darpa's space history. *Success Stories in Satellite Systems*, 10.2514/4.479670:353–378, 2009.

[17] S. H. Walker and F. Rodgers. Falcon hypersonic technology overview. (*AIAA*) *13th International Space Planes and Hypersonics Systems and Technologies*, 2005.

[18] L. Jinglin; C. Wanchun and M. Changwan. Steady glide reentry trajectory optimization with waypoint and no-fly zone constraints. (*IEEE*) *International Conference on Mechatronics and Automation*, pages 1363–1368, 2016.

DOI: 10.13009/EUCASS2017-545

[19] Y. Wu X. Z. Gao and X. Wang. Trajectory optimization in reentry phase for hypersonic gliding vehicles using swarm intelligence algorithms. *Practical applications of intelligent systems proceedings of the sixth international conference on intelligent systems and knowledge engineering*, pages 361–371, 2011.

[20] N. Yokoyama and S. Suzuki. Modified genetic algorithm for constrained trajectory optimization. *Journal of Guidance, Control, and Dynamics*, 28(1):139–144, 2005.

[21] K. Zhang. On-board three-dimensional trajectory planning for reentry vehicle. (*AIAA*) *20th International Space Planes and Hypersonic Systems and Technologies Conference*, 2015.

[22] K. Zhang and W. Chen. Reentry vehicle constrained trajectory optimization. (*AIAA*) *17th International Space Planes and Hypersonic Systems and Technologies Conference*, 2011.